

Three- to two-dimensional crossover in time-dependent density-functional theory

Shahrzad Karimi and Carsten A. Ullrich

Department of Physics and Astronomy, University of Missouri-Columbia, Columbia, Missouri, 65211

(Dated: January 20, 2020)

Quasi-two-dimensional (2D) systems, such as an electron gas confined in a quantum well, are important model systems for many-body theories. Earlier studies of the crossover from 3D to 2D in ground-state density-functional theory showed that local and semilocal exchange-correlation functionals which are based on the 3D electron gas are appropriate for wide quantum wells, but eventually break down as the 2D limit is approached. We now consider the dynamical case and study the performance of various linear-response exchange kernels in time-dependent density-functional theory. We compare approximate local, semilocal and orbital-dependent exchange kernels, and analyze their performance for inter- and intrasubband plasmons as the quantum wells approach the 2D limit. 3D (semi)local exchange functionals are found to fail for quantum well widths comparable to the 2D Wigner-Seitz radius r_s^{2D} , which implies in practice that 3D local exchange remains valid in the quasi-2D dynamical regime for typical quantum well parameters, except for very low densities.

PACS numbers: 31.15.ee, 31.15.ej, 71.45.Gm, 73.21.Fg

I. INTRODUCTION

The key concept of density-functional theory (DFT)¹ is that all electronic many-body systems can be uniquely characterized by their electron density $n(\mathbf{r})$. The density can be obtained in principle exactly via the Kohn-Sham equation (here and in the following we use atomic units),²

$$\left[-\frac{\nabla^2}{2} + v_0(\mathbf{r}) + v_H[n](\mathbf{r}) + v_{xc}[n](\mathbf{r}) \right] \varphi_j(\mathbf{r}) = \varepsilon_j \varphi_j(\mathbf{r}), \quad (1)$$

where $v_0(\mathbf{r})$ is a given external potential, $v_H[n](\mathbf{r}) = \int d^3r' n(\mathbf{r}')/|\mathbf{r}-\mathbf{r}'|$ is the Hartree potential, and $v_{xc}[n](\mathbf{r})$ is the exchange-correlation (xc) potential. The density is obtained from the self-consistent solution of Eq. (1) as $n(\mathbf{r}) = \sum_{j=1}^N |\varphi_j(\mathbf{r})|^2$, where N is the number of electrons, and all physical observables follow therefrom.

The xc potential is defined as the functional derivative $v_{xc}[n](\mathbf{r}) = \delta E_{xc}[n]/\delta n(\mathbf{r})$. The xc energy $E_{xc}[n]$ is a *universal* functional of the density: this means that there is one and only one exact density functional of the xc energy that is valid for *all* electronic systems with a given form of the electron-electron interaction, for any N . If this exact xc functional were known, it would give exact ground-state results, via Eq. (1), for all conceivable forms of matter, including atoms, molecules, and periodic or non-periodic solids.

In real matter, $v_0(\mathbf{r})$ consists of the Coulomb potentials of positively charged atomic nuclei. But the universality of $E_{xc}[n]$ and $v_{xc}[n](\mathbf{r})$ extends beyond real matter, and includes all mathematically reasonable forms of $v_0(\mathbf{r})$, whether they exist in nature or not. In particular, it includes systems of lower dimensionality, for instance electrons confined in a two-dimensional (2D) plane.³

A stringent test for approximate xc functionals is their performance during a dimensional crossover. The crossover from 3D to 2D has been previously studied in the DFT literature.⁵⁻⁸ It was found that local and semilocal functionals such as the local-density approximation

(LDA) and generalized gradient approximations (GGAs) fail badly at this task. To see this, consider the LDA exchange energy

$$E_{x,3D}^{LDA}[n] = -\frac{3}{4} \left(\frac{3}{\pi} \right)^{1/3} \int d^3r n(\mathbf{r})^{4/3}. \quad (2)$$

What happens if we try to evaluate $E_{x,3D}^{LDA}[n]$ for a 2D system? Let the density be $n_{2D}(\mathbf{r}) = n(\mathbf{r}_{||})\delta(z)$, where $\mathbf{r}_{||} = (x, y)$ denotes a 2D position vector. Using the delta function in the form $\delta(z) = \lim_{\epsilon \rightarrow 0^+} (4\pi\epsilon)^{-1/2} e^{-z^2/4\epsilon}$, one finds

$$E_{x,3D}^{LDA}[n_{2D}] = \lim_{\epsilon \rightarrow 0^+} \frac{3^{11/6}}{4^{5/3} \sqrt{\pi} \epsilon^{1/6}} \int d^2r_{||} n(\mathbf{r}_{||})^{4/3}. \quad (3)$$

This clearly shows that the 3D form of the LDA exchange energy diverges in the 2D limit, instead of approaching the proper form of the 2D LDA,⁴

$$E_{x,2D}^{LDA}[n] = -\frac{4}{3} \sqrt{\frac{2}{\pi}} \int d^2r_{||} n(\mathbf{r}_{||})^{3/2}. \quad (4)$$

All standard 3D GGAs will exhibit a similar divergence in the 2D limit.

To capture the 3D-2D crossover correctly, nonlocal xc functionals are needed. Some improvement over LDA and GGAs can be achieved with meta-GGA and hyper-GGA xc functionals,^{7,8} but only fully nonlocal xc functionals such as the average density approximation⁶ or the inhomogeneous STLS^{9,10} show a proper behavior as the 2D limit is approached.

In this paper, we extend the study of the dimensional crossover into the domain of time-dependent density-functional theory (TDDFT).¹¹⁻¹³ However, we will not explore the full dynamical range of TDDFT, which allows one to study electronic systems under the influence of arbitrary external time-dependent potentials, $v(\mathbf{r}, t)$; instead, we will limit ourselves to the linear-response regime and consider electronic excitation energies.^{14,15}

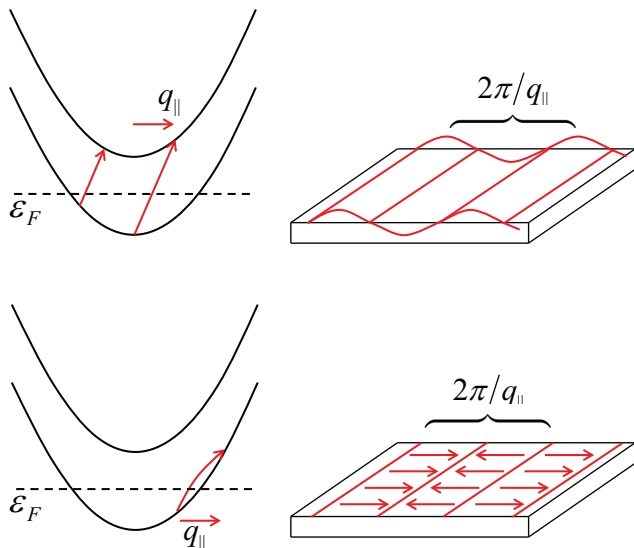


FIG. 1. Illustrations of intersubband (top) and intrasubband (bottom) plasmon excitations with wavevector q_{\parallel} in a quantum well with conduction band Fermi level ε_F in the lowest subband. Intersubband plasmons involve collective transitions between two subbands, leading to density oscillations of the quasi-2D electron system perpendicular to the quantum well plane. Intrasubband plasmons (collective transitions within the lowest subband) are characterized by density oscillations and currents flowing along the plane.

Furthermore, in this paper we will only consider exchange, but not correlation effects.

The main questions are the following. What characteristic effects or signatures occur in the excitation spectrum of a system as it crosses over from three to two dimensions, and how will the expected failure of LDA and GGA manifest itself? Will the breakdown be as drastic as in ground-state DFT, or will it perhaps be less severe, under some circumstances? How do nonlocal orbital functionals perform under the 3D-2D crossover?

Apart from the inherent fundamental interest, there are important practical reasons that motivate such a study. Quasi-2D¹⁶ electron gases (2DEGs) can be prepared in very high quality along interfaces and in heterostructures of a wide range of materials (most notably semiconductors and oxides), with many practical applications.^{17,18} It is important to be able to model the electronic structure and dynamics in these systems accurately and numerically efficiently. Since no DFT method beats the LDA in terms of simplicity and efficiency, one would like to know whether the 3D LDA is reliable in the quasi-2D regime, and under what circumstances it starts to fail. We will answer these questions in the following.

Figure 1 illustrates the two types of collective excitations that we will study in this paper. In a quantum well, electrons are free to move in the plane, but the levels are quantized into subbands due to quantum confinement perpendicular to the plane. Intersubband plas-

mons involve transitions from occupied to empty subbands; since different subbands have different envelope functions, this implies density oscillations *perpendicular* to the well plane. By contrast, intrasubband plasmons involve transitions within a subband; the accompanying currents and density oscillations are *parallel* to the plane. We will study what happens to these excitations as the quantum well becomes more and more narrow, approaching the strictly 2D limit.

This paper is organized as follows. In Section II we discuss the necessary theoretical background: we introduce our quantum well model, review the TDDFT linear-response formalism for collective excitations in quantum wells, and list various exchange functionals. In Section III we present our results, and Section IV gives conclusions. Some technical details are given in the Appendix.

II. THEORETICAL BACKGROUND

A. Quantum well model

We consider n-doped semiconductor quantum wells of width L in which the electrons are confined along the z direction and free to move in the x - y plane. The number of electrons per unit area (the sheet density) is denoted by N_s . In the following, we assume that the material of the quantum well is GaAs, with effective mass $m^* = 0.067m$ and effective charge $e^* = e/\sqrt{13}$ (m and e are the free electron mass and charge). We choose units in which $e^* = m^* = \hbar = 1$. The effective Hartree unit of energy is 10.8 meV; the effective Bohr radius is 103 Å.

The quantum well is assumed to be confined within infinitely high barriers at $z = 0$ and $z = L$. We further assume that the solutions of the Kohn-Sham equation for the quantum well envelope functions^{17,18} have the standard particle-in-a-box form,

$$\varphi_j(z) = \sqrt{\frac{2}{L}} \sin\left(\frac{j\pi z}{L}\right), \quad j = 1, 2, 3, \dots, \quad (5)$$

with Kohn-Sham energies

$$\varepsilon_j = \frac{1}{2} \left(\frac{j\pi}{L}\right)^2. \quad (6)$$

The Kohn-Sham potential $v_s(z) = v_{\text{ext}}(z) + v_H(z) + v_{\text{xc}}(z)$ that gives rise to these solutions is an infinitely deep square-well potential. This means that for each L and N_s the external quantum well potential $v_{\text{ext}}(z)$ is chosen such that, if added to the Hartree and xc potentials $v_H(z)$ and $v_{\text{xc}}(z)$, the resulting sum is a constant for $0 < z < L$. Thanks to the Hohenberg-Kohn theorem,¹ a unique choice of such a $v_{\text{ext}}(z)$ is always possible in principle; further details of the ground-state potentials do not need to be specified in the following.

We emphasize that the particle-in-a-box form of the Kohn-Sham eigenstates is only a matter of convenience,

and does not lead to a loss of generality of the results of the 3D-2D crossover that we study in this paper.

The ground-state density in the well is given by

$$n_0(z) = \frac{1}{\pi} \sum_{\substack{j \\ \varepsilon_j < \varepsilon_F}} \varphi_j^2(z) (\varepsilon_F - \varepsilon_j). \quad (7)$$

To determine the Fermi energy ε_F , we integrate the density over z :

$$\int_0^L dz n_0(z) = N_s = \frac{1}{\pi} \sum_{j=1}^{N_{\text{occ}}} (\varepsilon_F - \varepsilon_j), \quad (8)$$

where N_{occ} is the number of occupied subbands. Hence,

$$\varepsilon_F = \frac{\pi N_s}{N_{\text{occ}}} + \frac{1}{N_{\text{occ}}} \sum_{j=1}^{N_{\text{occ}}} \varepsilon_j, \quad (9)$$

and N_{occ} is fixed by requiring $\varepsilon_{N_{\text{occ}}} < \varepsilon_F < \varepsilon_{N_{\text{occ}}+1}$.

B. Excitations within linear-response TDDFT

In the following, we are interested in the frequency-dependent spin-density response in a quantum well. Because of the translational symmetry in the $x - y$ plane, we Fourier transform with respect to the in-plane position vector $\mathbf{r}_{\parallel} = (x, y)$; this introduces the in-plane wavevector \mathbf{q}_{\parallel} . The TDDFT linear-response equation¹⁹ then becomes

$$n_{1\sigma}(\mathbf{q}_{\parallel}, z, \omega) = \int dz' \chi_{s\sigma\sigma}(\mathbf{q}_{\parallel}, z, z', \omega) v_{s1\sigma}(\mathbf{q}_{\parallel}, z', \omega). \quad (10)$$

The noninteracting response function is diagonal in the spin σ :

$$\begin{aligned} \chi_{s,\sigma\sigma'}(\mathbf{q}_{\parallel}, z, z', \omega) &= \delta_{\sigma\sigma'} \sum_{j=1}^{N_{\text{occ}}} \sum_{l=1}^{\infty} F_{lj}(\mathbf{q}_{\parallel}, \omega) \\ &\quad \times \varphi_j(z) \varphi_l(z) \varphi_j(z') \varphi_l(z'), \end{aligned} \quad (11)$$

where

$$\begin{aligned} F_{lj}(\mathbf{q}_{\parallel}, \omega) &= \int \frac{d^2 k_{\parallel}}{(2\pi)^2} \left[\frac{\theta(\varepsilon_F - \varepsilon_j - k_{\parallel}^2/2)}{\omega - \omega_{lj} - \mathbf{q}_{\parallel} \mathbf{k}_{\parallel} - q_{\parallel}^2/2 + i\eta} \right. \\ &\quad \left. - \frac{\theta(\varepsilon_F - \varepsilon_j - k_{\parallel}^2/2)}{\omega + \omega_{lj} + \mathbf{q}_{\parallel} \mathbf{k}_{\parallel} + q_{\parallel}^2/2 + i\eta} \right]. \end{aligned} \quad (12)$$

Here, $\omega_{jk} = \varepsilon_k - \varepsilon_j$, and η is a positive infinitesimal. The linearized effective potential, $v_{s1\sigma} = v_{1\sigma} + v_{\text{Hxc}1\sigma}$, consists of an external scalar perturbation plus a linearized Hartree-xc contribution:

$$\begin{aligned} v_{\text{Hxc}1\sigma}(\mathbf{q}_{\parallel}, z, \omega) &= \sum_{\sigma'} \int dz' \left[\frac{2\pi}{q_{\parallel}} e^{-q_{\parallel}|z-z'|} \right. \\ &\quad \left. + f_{\text{xc},\sigma\sigma'}(\mathbf{q}_{\parallel}, z, z', \omega) \right] n_{1\sigma'}(\mathbf{q}_{\parallel}, z', \omega). \end{aligned} \quad (13)$$

The xc kernel $f_{\text{xc},\sigma\sigma'}$ will be discussed in more detail below.

The following external perturbation triggers both single-particle and collective excitations with a finite in-plane wave vector \mathbf{q}_{\parallel} :

$$v_{1\sigma}(\mathbf{q}_{\parallel}, z, \omega) = S_{\sigma}^{\pm} E_0 e^{q_{\parallel} z}, \quad (14)$$

which couples to the charge (+) and the spin (−) channel via $S_{\sigma}^{\pm} = \delta_{\sigma,\uparrow} \pm \delta_{\sigma,\downarrow}$, respectively. Having solved the response equation (10) self-consistently, we obtain the absorption cross section as

$$\sigma(\mathbf{q}_{\parallel}, \omega) = -\frac{2\omega}{E_0 q_{\parallel}^2} \Im \sum_{\sigma} S_{\sigma}^{\pm} \int dz e^{q_{\parallel} z} n_{1\sigma}(\mathbf{q}_{\parallel}, z, \omega). \quad (15)$$

The absorption cross section, when plotted as a function of frequency, has peaks at those frequencies that are resonant with an excitation energy of the system; the peak height is a measure of the oscillator strength.

The alternative to calculating the absorption cross section is to directly calculate the excitation energies of the system. The idea is that an electronic excitation can be viewed as an electronic eigenmode, i.e., a dynamical response of the system that is self-sustained and does not require an external perturbation. The characteristic eigenmode frequencies are thus obtained as those frequencies Ω where the linear-response equation has a nontrivial solution in the absence of an external perturbation.^{13,14} The resulting general formalism for calculating excitation energies in TDDFT has the form of an eigenvalue equation:^{12,15}

$$\begin{pmatrix} \mathbf{A} & \mathbf{K} \\ \mathbf{K} & \mathbf{A} \end{pmatrix} \begin{pmatrix} \mathbf{X} \\ \mathbf{Y} \end{pmatrix} = \Omega \begin{pmatrix} -1 & 0 \\ 0 & 1 \end{pmatrix} \begin{pmatrix} \mathbf{X} \\ \mathbf{Y} \end{pmatrix}, \quad (16)$$

where the matrix elements of \mathbf{A} and \mathbf{K} are given by

$$\begin{aligned} A_{ia\sigma, i'a'\sigma'}(\omega) &= \delta_{ii'} \delta_{aa'} \delta_{\sigma\sigma'} \omega_{ai\sigma} + K_{ia\sigma, i'a'\sigma'}(\omega) \\ K_{ia\sigma, i'a'\sigma'}(\omega) &= \int d^3 r \int d^3 r' \varphi_i^*(\mathbf{r}) \varphi_a(\mathbf{r}) \left\{ \frac{1}{|\mathbf{r} - \mathbf{r}'|} \right. \\ &\quad \left. + f_{\text{xc}\sigma\sigma'}(\mathbf{r}, \mathbf{r}', \omega) \right\} \varphi_{i'}(\mathbf{r}') \varphi_{a'}^*(\mathbf{r}') \end{aligned} \quad (17)$$

and i, i' and a, a' run over occupied and unoccupied Kohn-Sham orbitals, respectively. In almost all applications of this formalism one uses frequency-independent approximations for the xc kernel.

Equation (16) can be adapted in a rather straightforward manner to calculate inter- and intrasubband charge and spin plasmon frequencies in quantum wells; all one needs to do is use the explicit form $\varphi_j(\mathbf{r}) = A^{-1/2} \varphi_j(z) e^{i\mathbf{k}_{\parallel} \cdot \mathbf{r}_{\parallel}}$ of the single-particle wave functions and then Fourier transform with respect to \mathbf{r}_{\parallel} .

Rather than giving the general formalism, let us consider the much simpler (but very important) quasi-2D case. Assume that only the lowest subband is occupied, and consider the lowest intersubband plasmon modes at wavevector $\mathbf{q}_{\parallel} = 0$. Ignoring the influence of the third

and higher subbands, the intersubband charge and spin plasmon frequencies are given by

$$\Omega_{c,s}^2 = \omega_{21}^2 + \omega_{21} N_s (K_{\uparrow\uparrow} \pm K_{\uparrow\downarrow}), \quad (19)$$

where

$$K_{\sigma\sigma'} = \int dz \int dz' \varphi_1(z) \varphi_2(z) [-2\pi|z - z'| + f_{xc,\sigma\sigma'}(z, z')] \varphi_1(z') \varphi_2(z'). \quad (20)$$

C. Exchange kernels

The main purpose of this paper is to compare the performance of different approximate xc kernels in the crossover from 3D to 2D. In the following we shall limit ourselves to the exchange-only case. For systems that are not spin polarized, the spin-resolved exchange kernel $f_{x,\sigma\sigma'}$ is obtained from the spin-unresolved exchange kernel f_x as

$$f_{x,\sigma\sigma'} = 2\delta_{\sigma\sigma'} f_x. \quad (21)$$

We compare three different frequency-independent exchange kernels: ALDA, PBE, and PGG. The ALDA exchange kernel is defined as follows:

$$f_x^{\text{ALDA}}(\mathbf{r}, \mathbf{r}') = \frac{d^2 e_x^h(\bar{n})}{d\bar{n}^2} \Big|_{\bar{n}=n(\mathbf{r})} \delta(\mathbf{r} - \mathbf{r}'), \quad (22)$$

where $e_x^h(n)$ is the exchange energy density of a homogeneous electron liquid of density n .⁴ Hence, the 3D and 2D ALDA exchange kernels are given by

$$f_{x,3D}^{\text{ALDA}}(\mathbf{r}, \mathbf{r}') = -[9\pi n^2(\mathbf{r})]^{-1/3} \delta(\mathbf{r} - \mathbf{r}') \quad (23)$$

$$f_{x,2D}^{\text{ALDA}}(\mathbf{r}_{||}, \mathbf{r}'_{||}) = -[\pi n_{2D}(\mathbf{r}_{||})/2]^{-1/2} \delta(\mathbf{r}_{||} - \mathbf{r}'_{||}). \quad (24)$$

The PBE functional²⁰ is probably the most widely used GGA; it is defined only for 3D systems. The explicit expression for the PBE exchange kernel turns out to be quite lengthy, and is given in Appendix A.

In contrast with ALDA and PBE, the so-called PGG functional^{14,21} is a nonlocal orbital functional, given by

$$f_x^{\text{PGG}}(\mathbf{r}, \mathbf{r}') = -2 \frac{\left| \sum_{j=1}^{N_{\text{occ}}} \varphi_j(\mathbf{r}) \varphi_j^*(\mathbf{r}') \right|^2}{|\mathbf{r} - \mathbf{r}'| n(\mathbf{r}) n(\mathbf{r}')}, \quad (25)$$

where the sum runs over N_{occ} doubly occupied orbitals. PGG can be viewed as an approximation to the exact exchange kernel.¹² We give the explicit form of the PGG kernel for quasi-2D systems and for the 2D limit in Appendix B, and discuss its relation to exchange-only ISTLS in Appendix C.

III. RESULTS AND DISCUSSIONS

A. Plasmons: from bulk to quasi-2D

Plasmons in homogeneous electron liquids have been thoroughly studied for many decades.²² The plasmon dispersions in 2D and 3D follow from the exact conditions

$$\left[\frac{4\pi}{q^2} + f_{xc,3D}(q, \Omega_{3D}) \right] \chi_0^{3D}(q, \Omega_{3D}) = 1 \quad (26)$$

$$\left[\frac{2\pi}{q_{||}} + f_{xc,2D}(q_{||}, \Omega_{2D}) \right] \chi_0^{2D}(q_{||}, \Omega_{2D}) = 1, \quad (27)$$

where $\chi_0^{3D}(q, \Omega)$ and $\chi_0^{2D}(q_{||}, \Omega)$ are the 3D and 2D Lindhard functions.⁴ In the limit of small wavevectors, one obtains

$$\Omega_{3D}(q \rightarrow 0) = \omega_{\text{pl}} \left[1 + \left(\frac{3(k_F^{3D})^2}{10\omega_{\text{pl}}^2} + \frac{f_{xc,3D}(0, \omega_{\text{pl}})}{8\pi} \right) q^2 \right], \quad (28)$$

where $\omega_{\text{pl}} = \sqrt{4\pi n}$ is the classical plasma frequency of a 3D electron liquid of density n , and k_F^{3D} is the associated Fermi wavevector. The corresponding relation in 2D is

$$\Omega_{2D}(q_{||} \rightarrow 0) = k_F^{2D} \sqrt{q_{||}} \left[1 + \frac{q_{||}}{2\pi} f_{xc,2D}(0, 0) \right]^{1/2}. \quad (29)$$

$\Omega_{3D}(q)$ and $\Omega_{2D}(q_{||})$ both describe charge plasmons (i.e., collective oscillations of the charge density n). There are no corresponding 3D and 2D spin plasmons (i.e., collective oscillations of the spin density) as long as the system is not magnetic: the reason is that the 3D and 2D spin plasmons fall into the respective particle-hole continua and are hence Landau damped.

Suppose now that we start from a homogeneous 3D system and let one of its dimensions, say z , become confined: this defines a neutral jellium slab.^{23,24} Let us consider a jellium slab that corresponds to the quantum well model with hard boundaries that we described in Section II.A. What happens to the plasmon mode as the width L of this system shrinks down to the quantum limit?

As soon as L becomes finite, the collective excitations are described using the formalism of intersubband plasmons. We consider the case where the average 3D density \bar{n} in the well is constant, letting

$$\bar{n} = N_s/L. \quad (30)$$

If L is very large, the difference between two consecutive energy levels ε_j and ε_{j+1} , see Eq. (6), is very small, and a large number of subbands is occupied. As L shrinks, the level spacing increases and fewer and fewer subbands are occupied. Let L_ν be that width where the Fermi energy ε_F coincides with the ν th level ε_ν . From Eqs. (6) and (9) it is straightforward to show that

$$L_\nu^3 = \frac{\pi\nu}{12\bar{n}} (4\nu^2 - 3\nu - 1), \quad (31)$$

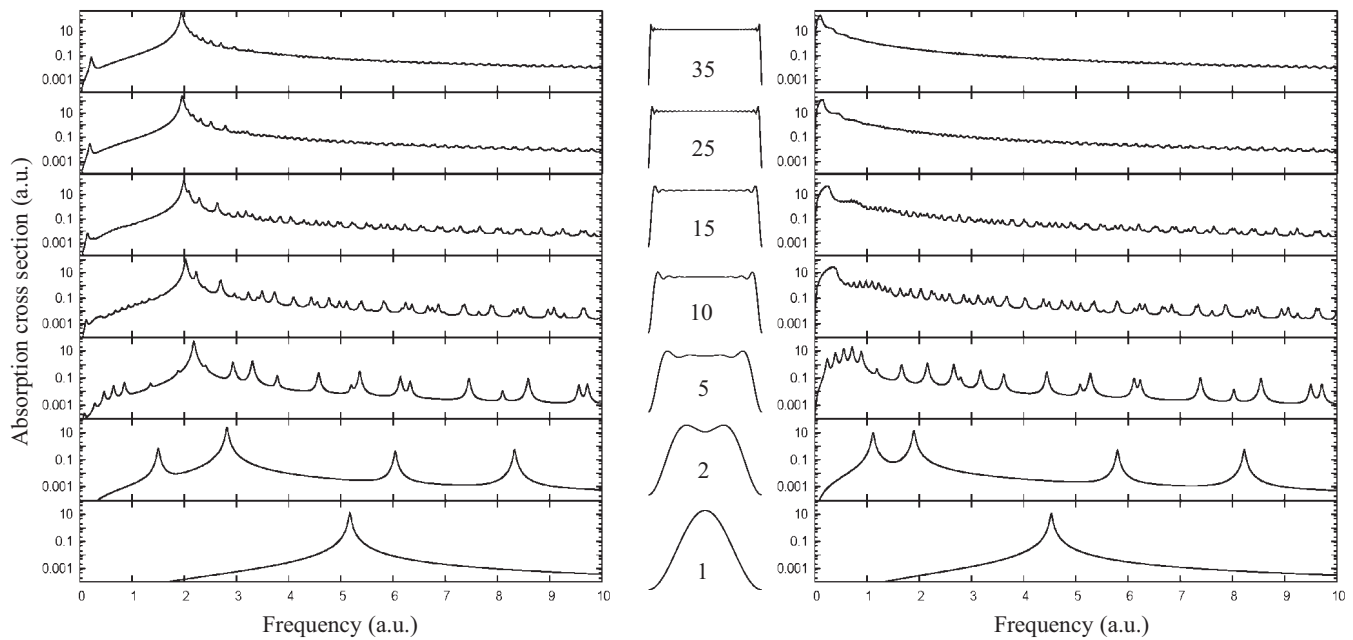


FIG. 2. Photoabsorption cross section for $q_{\parallel} = 0$ intersubband excitations in quantum wells. Left panels: charge-density excitations. Right panels: spin-density excitations. Insets: density profiles at given values of N_{occ} . The calculations were done with the 3D ALDA exchange kernel.

where we used $\sum_{j=1}^{\nu} j^2 = \nu(\nu+1)(2\nu+1)/6$. In particular, for $\nu = 2$ we have

$$L_2 = \left(\frac{3\pi}{2\bar{n}} \right)^{1/3}. \quad (32)$$

For $L < L_2$, only the lowest subband is occupied (the quantum limit). Equation (32) can also be rewritten in terms of the 2D Wigner-Seitz radius r_s^{2D} as⁵

$$L_2 = \sqrt{\frac{3\pi}{2N_s}} = \pi r_s^{2D} \sqrt{\frac{3}{2}} \approx 3.85 r_s^{2D}. \quad (33)$$

Figure 2 shows ALDA intersubband excitation spectra at $q_{\parallel} = 0$, in the charge and spin channel, for quantum wells with different numbers of occupied subbands, ranging from $N_{\text{occ}} = 1$ to 35. L and N_s are chosen such that the average density remains constant at $\bar{n} = 0.30 a_0^{*-3}$. The insets in the middle show how the density profile becomes more and more square shaped as N_{occ} increases.

In the quasi-2D limit where $N_{\text{occ}} = 1$, the spectra only show a single peak in the energy range below 10 a.u.: the intersubband charge plasmon at 5.17 a.u. (left bottom panel) and spin plasmon at 4.53 a.u. (right bottom panel). As more subbands become occupied, the spectra acquire more and more peaks, and eventually approach very simple limits for large N_{occ} .

At $N_{\text{occ}} = 35$, the charge-density excitation spectrum is dominated by a single peak at 1.94 a.u., which is the bulk plasmon frequency ω_{pl} corresponding to \bar{n} . There is also a small peak around 0.22 a.u., which corresponds to

the surface plasmon of a large jellium slab with a sharp density profile.²⁵ On the other hand, the spin-density excitation spectrum has become essentially featureless; in other words, the spin plasmon has disappeared, as expected.

Thus, there is a seamless transition between the 3D bulk plasmon and the intersubband plasmons as the 2D limit is approached. In this regime, the 3D ALDA (or any 3D semilocal functional) is appropriate.

B. 2D Limit of intersubband plasmons

We now focus on the situation where only the first subband is occupied ($N_{\text{occ}} = 1$), i.e., we consider quantum wells of width $L < L_2$. Figure 3 shows the intersubband charge and spin plasmon dispersions for quantum wells with $N_s = 10^{12} \text{ cm}^{-2}$ and $L = 100$ and 40 \AA , respectively, calculated with RPA, ALDA, PBE and PGG. In all cases, the charge plasmon dispersion lies above the spin plasmon dispersion (except for RPA, which has no spin plasmon). However, the position of the intersubband plasmon dispersions relative to the particle-hole (p-h) continuum varies.

For the 100 \AA wide quantum well we find that the charge plasmon branches are above the p-h continuum and spin plasmon branches are below. For the 40 \AA well, however, the charge plasmon branch has moved *below*²⁶ the p-h continuum for ALDA and PBE, but not for RPA and PGG. This is a remarkable difference between semilo-

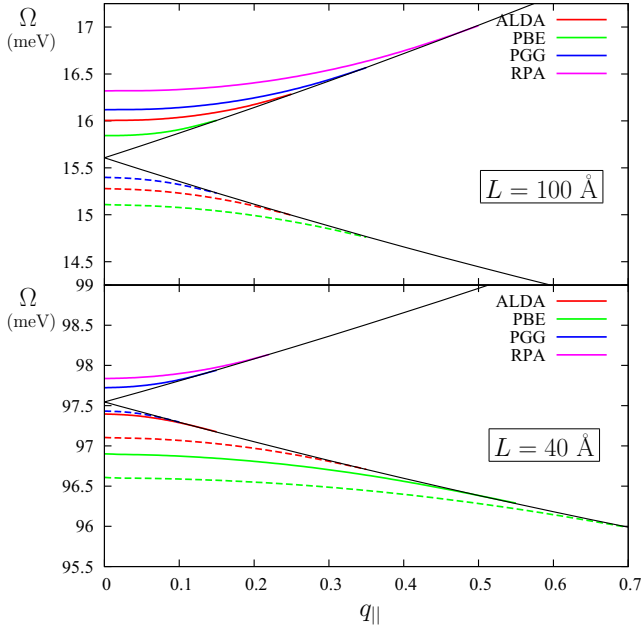


FIG. 3. (Color online) Intersubband plasmon dispersions $\Omega(q_{\parallel})$, for $N_s = 10^{12} \text{ cm}^{-2}$ and well widths 100 Å and 40 Å. The black full lines indicate the intersubband p-h continuum. The RPA only gives intersubband charge plasmons; ALDA, PBE and PGG give both charge (full lines) and spin plasmons (dashed lines). ALDA and PBE break down when their charge plasmons falls below the p-h continuum.

cal and orbital-dependent exchange functionals, and we will now investigate this effect in more detail.

Let us consider the case $q_{\parallel} = 0$ and keep the sheet density N_s fixed. As $L \rightarrow 0$, the system transitions from quasi-2D to strictly 2D.¹⁶ In this limit, the intersubband excitation energies become infinitely large, because the system is so strongly confined in the plane that density fluctuations perpendicular to the quantum well plane (see Fig. 1) become impossible. However, it is interesting to observe how the intersubband plasmons behave as this limit is approached. This is shown in Fig. 4.

We have calculated the $q_{\parallel} = 0$ intersubband charge and spin plasmon energies with RPA (charge plasmon only), ALDA, PBE, and PGG. According to Eq. (6) the lowest p-h transition energy is $\omega_{21} = 3\pi^2/2L^2$. Hence, $\omega_{21}L^2$ is constant, as indicated by the thin horizontal line in Fig. 4. As L becomes smaller, the plasmon energies (scaled by L^2) approach and eventually merge with the p-h line.

The RPA plasmon energy follows from Eq. (19) as

$$(\Omega_c^{\text{RPA}} L^2)^2 = \frac{9\pi^4}{4} + \frac{20\pi N_s L^3}{3}, \quad (34)$$

where the Hartree part of the intersubband matrix ele-

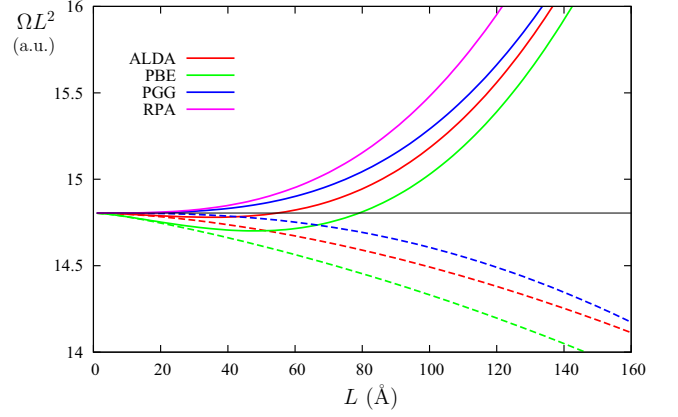


FIG. 4. (Color online) Intersubband plasmon energies, at $q_{\parallel} = 0$, versus well width L , for $N_s = 10^{12} \text{ cm}^{-2}$. The horizontal line indicates the lowest p-h transition ω_{21} (all energies are scaled by L^2). The RPA only gives intersubband charge plasmons; ALDA, PBE and PGG give both charge (full lines) and spin plasmons (dashed lines). ALDA and PBE break down when the charge plasmon falls below the p-h line.

ment (20) is given by

$$-2\pi \int dz \int dz' \varphi_1(z) \varphi_2(z) |z - z'| \varphi_1(z') \varphi_2(z') = \frac{20L}{9\pi}. \quad (35)$$

Hence, the RPA charge plasmons are always shifted *above* the p-h line, but the separation vanishes as $L \rightarrow 0$.

In ALDA, we find

$$(\Omega_c^{\text{ALDA}} L^2)^2 = \frac{9\pi^4}{4} + \frac{20\pi N_s L^3}{3} - c_1 (48\pi^2 N_s L^5)^{1/3} \quad (36)$$

$$(\Omega_s^{\text{ALDA}} L^2)^2 = \frac{9\pi^4}{4} - c_1 (48\pi^2 N_s L^5)^{1/3}, \quad (37)$$

where $c_1 = \int_0^\pi dx \sin^2(2x) \sin^{2/3}(x) = 1.20027$. For the PBE and PGG plasmon energies no simple analytic expressions exist; however, numerical evaluation is straightforward using the formulas in the Appendix.

As can be seen from Fig. 4, the ALDA and PBE charge plasmons cross over the p-h line: this happens at $L = 54.6 \text{ Å}$ in ALDA and at $L = 79 \text{ Å}$ in PBE. No such crossover is observed for PGG.

The critical width $L_{\text{crit}}^{\text{inter}}$ at which the crossover occurs in ALDA and PBE is plotted in Fig. 5 as a function of the sheet density N_s . In ALDA we can use Eq. (36) to find the analytical result

$$L_{\text{crit}}^{\text{inter}} = \frac{3c_1^{3/4}}{5\sqrt{N_s}} \left(\frac{5}{4\pi} \right)^{1/4} = \frac{0.546}{\sqrt{N_s}} \text{ a.u.} \quad (38)$$

For PBE, we obtain numerically $L_{\text{crit}}^{\text{inter}} = 0.79/\sqrt{N_s}$ a.u. In terms of the 2D Wigner-Seitz radius, this becomes $L_{\text{crit}}^{\text{inter}} = 0.975 r_s^{2\text{D}}$ and $1.40 r_s^{2\text{D}}$ for ALDA and PBE, respectively. In the case of ALDA, this is about 4 times smaller than L_2 [Eq. (33)], the width of the quantum

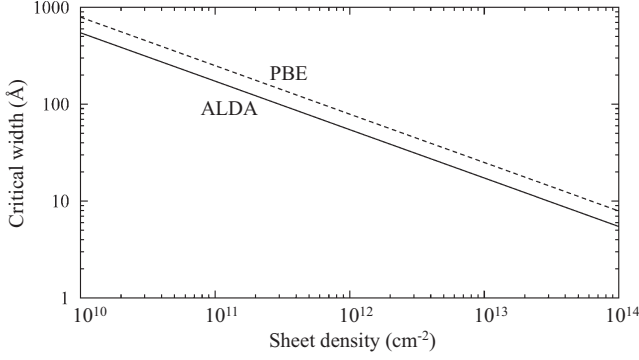


FIG. 5. Critical width $L_{\text{crit}}^{\text{inter}}$ at which the intersubband plasmon breakdown occurs, as a function of sheet density N_s . Full line: ALDA, dashed line: PBE.

well below which only the lowest subband is occupied; in the case of PBE, it is about 3 times smaller.

In PGG, we find that the charge and spin plasmons always lie above and below the p-h continuum, respectively. This is similar to the case of excitation energies in atoms, where the bare Kohn-Sham excitations are found to lie between the singlet and triplet excitations.^{27–29} Hence, the crossover of ALDA and PBE indicates a general failure of semilocal functionals in the 2D limit of intersubband transitions.

However, it is important to note that this failure does not appear to be a catastrophic breakdown, as in the case of the diverging exchange energy that we discussed in the Introduction. The intersubband plasmons may have a wrong position with respect to the p-h continuum, but they still exist as collective modes, and deviate not too far from the PGG results. Furthermore, the separation between charge and spin plasmons (the analog of the singlet-triplet splitting in atoms) remains well described in ALDA and PBE for all L .

In practice, the width of quantum wells is limited by the underlying material (for GaAs, the lattice constant is 5.65 Å). Typical semiconductor quantum wells have widths of several hundreds of Å, so that one is usually sufficiently far away from the critical widths where the ALDA breaks down for the intersubband dynamics, except for situations where N_s is very small.

C. 2D limit of intrasubband plasmons

Let us now consider the intrasubband plasmons in a quantum well with $N_{\text{occ}} = 1$, in the limit where $L \rightarrow 0$. For convenience, we shift the bottom of the quantum well potential such that the lowest subband level $\varepsilon_1 = 0$. Assuming, furthermore, that the second and higher subband levels are energetically well separated from the lowest subband, the response function (11) is given by

$$\chi_{s,\sigma\sigma'}(\mathbf{k}_{\parallel}, z, z', \omega) = \delta_{\sigma\sigma'} \Phi(z, z') \chi_0^{2\text{D}}(k_{\parallel}, \omega), \quad (39)$$

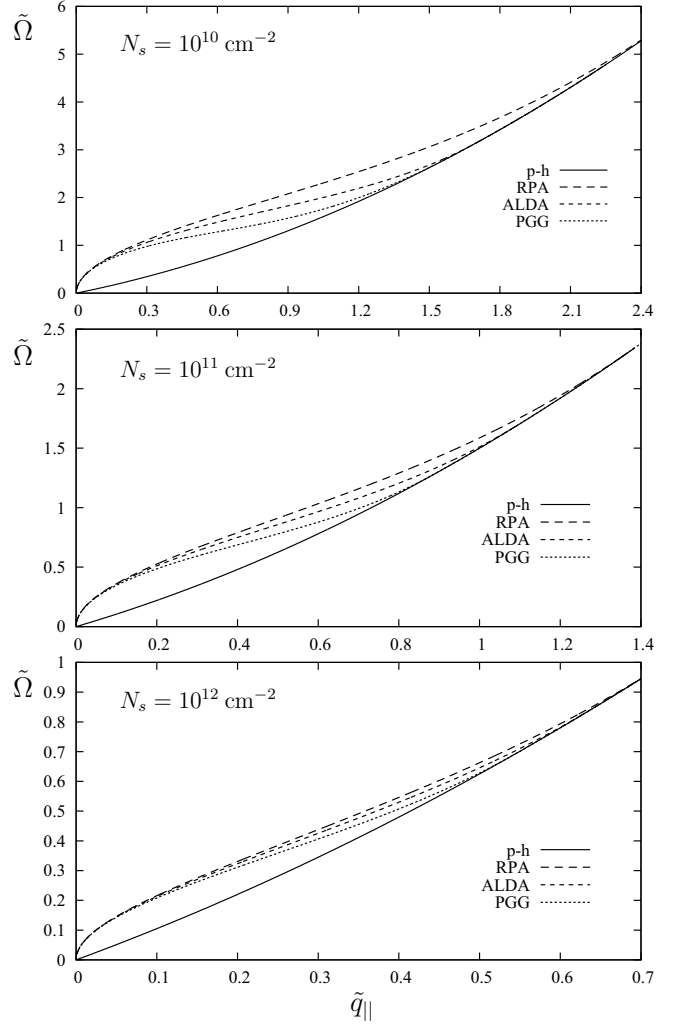


FIG. 6. Plasmon dispersions $\Omega(q_{\parallel})$ for strictly 2D systems with sheet densities $N_s = 10^{10}$, 10^{11} , and 10^{12} cm^{-2} , calculated with RPA, 2D ALDA and PGG. The full lines denote the upper boundaries of the particle-hole (p-h) continuum. Here, $\tilde{q}_{\parallel} = q_{\parallel}/k_F^{2\text{D}}$ and $\tilde{\Omega} = \Omega/(k_F^{2\text{D}})^2$.

where $\chi_0^{2\text{D}}(k_{\parallel}, \omega)$ is the 2D Lindhard function, and where we abbreviate $\Phi(z, z') = \varphi_1^2(z)\varphi_1^2(z')$. The response equation (10) for the eigenmodes then becomes

$$n_1(q_{\parallel}, z', \Omega) = \int dz_1 \Phi(z', z_1) \chi_0^{2\text{D}}(q_{\parallel}, \Omega) \times \int dz_2 f_{\text{Hxc}}(q_{\parallel}, z_1, z_2) n_1(q_{\parallel}, z_2, \Omega). \quad (40)$$

Multiply both sides with $\varphi_1^2(z) f_{\text{Hxc}}(q_{\parallel}, z, z')$ and integrate over z and z' . Then, n_1 cancels out and we are left with the condition

$$1 = \int dz \int dz' \Phi(z, z') \left[\frac{2\pi}{q_{\parallel}} e^{-q_{\parallel}|z-z'|} + f_{\text{xc}}(z, z') \right] \times \chi_0^{2\text{D}}(q_{\parallel}, \Omega). \quad (41)$$

The intrasubband plasmons of the quasi-2D quantum well are those frequencies Ω where Eq. (41) is satisfied. The question is now this: if $L \rightarrow 0$, will Eq. (41) turn into Eq. (27) for the 2D plasmons?

A straightforward calculation shows that this is indeed the case for the Hartree part, as expected. Using the particle-in-a-box wave function (5) we obtain

$$\int dz \int dz' \Phi(z, z') e^{-q_{||}|z-z'|} = \frac{q_{||}L}{(q_{||}^2 L^2 + 4\pi^2)^2} \times \left\{ 3q_{||}^2 L^2 + 20\pi^2 + \frac{32\pi^4}{q_{||}^3 L^3} (e^{-q_{||}L} - 1 + q_{||}L) \right\} \rightarrow 1 \quad \text{for } L \rightarrow 0. \quad (42)$$

For the PGG exchange kernel, it is straightforward to show that

$$\int dz \int dz' \Phi(z, z') f_x^{\text{PGG}}(q_{||}, z, z') \rightarrow f_{x,2\text{D}}^{\text{PGG}}(q_{||}) \quad (43)$$

for $L \rightarrow 0$, where $f_x^{\text{PGG}}(q_{||}, z, z')$ and $f_{x,2\text{D}}^{\text{PGG}}(q_{||})$ are given in Appendix B, see Eqs. (B4 and (B6). Thus, the PGG exchange kernel behaves correctly in the 2D limit.

However, it is hardly surprising to find that the ALDA does not give the correct 2D limit. We have

$$\int dz \int dz' \Phi(z, z') f_{x,3\text{D}}^{\text{ALDA}}(z, z') = -\frac{2c_2}{3\pi} \left(\frac{6}{\pi L} \right)^{1/3} n_{2\text{D}}^{-2/3}, \quad (44)$$

where $c_2 = \int_0^\pi dx \sin^{8/3}(x) = 1.4003$. This clearly disagrees with the form of $f_{x,2\text{D}}^{\text{ALDA}} = -\sqrt{2/\pi n_{2\text{D}}}$, and in fact diverges as $L \rightarrow 0$. Other semilocal functionals such as PBE show similar trends.

Figure 6 shows the plasmon dispersions in the strictly 2D limit, calculated by solving Eq. (27). The ALDA and PGG calculations were done with the 2D exchange kernels $f_{x,2\text{D}}^{\text{ALDA}}$ and $f_{x,2\text{D}}^{\text{PGG}}$, respectively. The upper boundary of the particle-hole continuum is given by the relation $\Omega_{p-h} = \tilde{q}_{||}^2/2 + \tilde{q}_{||}$, where $\tilde{q}_{||} = q_{||}/k_F^{2\text{D}}$. One observes that the RPA plasmon dispersion always lies above ALDA and PGG, reflecting the downshift of excitation energies caused by exchange.

Figure 7 compares the intrasubband plasmon dispersions of PGG and 3D ALDA for well widths $L = \lambda L_2$, where we let the scaling parameter λ take on values between 1 and 0.001 [recall that L_2 , Eq. (32), is the maximum well width for which only the lowest subband is occupied for a given N_s]. The sheet density is $N_s = 10^{10} \text{ cm}^{-2}$, and we have $L_2 = 217 \text{ nm}$.

As expected, PGG nicely approaches the 2D limit that was shown in Fig. 6. For $\lambda < 0.01$, the intrasubband plasmon dispersion becomes indistinguishable from the strictly 2D limit.

The situation is drastically different for the ALDA. As λ decreases from 1 to 0.1, the intrasubband dispersion appears to approach the 2D limit. However, below $\lambda = 0.1$ the 3D ALDA breaks down, and the intrasubband plasmon dispersion becomes more and more suppressed, that

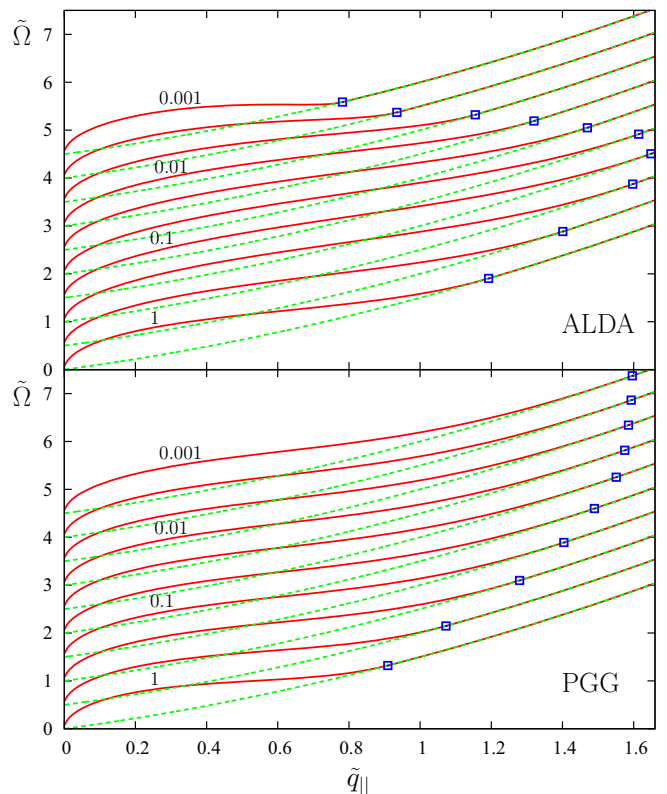


FIG. 7. (Color online) Intrasubband plasmon dispersions for quantum wells with sheet density $N_s = 10^{10} \text{ cm}^{-2}$, for different widths $L = \lambda L_2$, where λ takes on the values 1, 0.5, 0.2, 0.1, 0.05, 0.02, 0.01, 0.005, 0.002, and 0.001. $L_2 = 217 \text{ nm}$ is the largest width for which only the lowest subband is occupied. The individual plasmon dispersions are offset for clarity. The dashed lines are the upper boundaries of the p-h continuum. The squares indicate the wavevector $\tilde{q}_{||p-h}$ where the plasmons enter the p-h continuum. Top panel: 3D ALDA. Bottom panel: PGG.

is, it begins to merge with the p-h continuum at smaller and smaller wavevectors. As $\lambda \rightarrow 0$, the intrasubband plasmon completely disappears, rather than approaching the 2D plasmon shown in Fig. 6.

We have repeated these calculations for several different values of the sheet density N_s , focusing on the wavevector $\tilde{q}_{||p-h}$ where the intrasubband plasmon enters the p-h continuum, as indicated by the blue squares in Fig. 7.

Figure 8 shows $\tilde{q}_{||p-h}$ versus the well width scaling factor λ for $N_s = 10^{10}, 10^{11}, 10^{12}$, and 10^{13} cm^{-2} , calculated with ALDA and PGG. For PGG we see in each case that $\tilde{q}_{||p-h}$ smoothly approaches its limiting value for the strictly 2D plasmon, shown by the dashed line. The ALDA initially approaches the 2D limit as λ decreases from 1. However, around $\lambda = 0.1$ all ALDA curves turn around and rapidly drop off, moving away from the 2D limit.

Thus, we find that the 3D ALDA exchange kernel be-

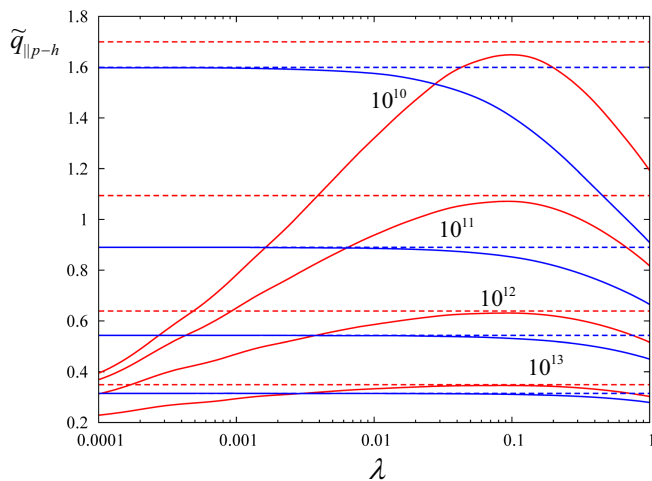


FIG. 8. (Color online) Wavevector $\tilde{q}_{\parallel p-h}$ at which the intrasubband plasmon merges with the p-h continuum, plotted versus well width scaling factor λ , calculated with PGG (blue) and ALDA (red). The dashed lines indicate the respective limits for the strictly 2D case. The calculations were done for sheet densities $N_s = 10^{10}, 10^{11}, 10^{12}$, and 10^{13} cm^{-2} , as indicated. The breakdown of the 3D ALDA occurs around $\lambda = 0.1$ for all N_s .

has reasonably as long as the well width is sufficiently large. The breakdown for intrasubband (in-plane) dynamics occurs for $L_{\text{crit}}^{\text{intra}} \approx 0.1L_2 \approx 0.4r_s^{2D}$. Interestingly, this is significantly smaller than the critical intersubband width $L_{\text{crit}}^{\text{inter}} \approx r_s^{2D}$, see Section III.B.

IV. CONCLUSIONS

In this paper we have carried out systematic numerical studies of the electron dynamics in quantum wells whose width L crosses over from the 3D to the quasi-2D regime (where only the lowest subband is occupied, but the finite size is still relevant) and finally to the strictly 2D limit (where $L = 0$). The purpose was a comparison of different classes of exchange kernels in TDDFT: standard semilocal kernels (such as ALDA and PBE) and nonlocal kernels (such as PGG and ISTLS). ALDA and PBE are based on the electron gas as reference system, whereas PGG and ISTLS are orbital functionals, whose definition does not invoke any reference system.

The main conclusion does not come as a surprise: ALDA and PBE fail in the 3D-2D crossover, PGG succeeds. This is already well known for the ground state,⁵⁻⁸ and there was no reason to expect otherwise for the dynamical case. However, the details are interesting and of practical relevance.

First of all, we discover a universal behavior of the breakdown of the inter- and intrasubband dynamics in 3D ALDA. At a critical well width of $L_{\text{crit}}^{\text{inter}} \approx r_s^{2D}$, intersubband plasmons are no longer qualitatively cor-

rectly described (the charge plasmon falls below the single-particle excitation ω_{21}). For well widths below $L_{\text{crit}}^{\text{intra}} \approx 0.4r_s^{2D}$, intrasubband plasmon dispersions start to become suppressed compared to the 2D limit. The interesting finding is thus that $L_{\text{crit}}^{\text{intra}} < L_{\text{crit}}^{\text{inter}}$, so the in-plane dynamics appears to be well described using the 3D ALDA down to much smaller widths than the out-of-plane dynamics.

Compared to the ground state, the failure of the (semi)local xc functionals in the dynamical case is of a different nature. In fact, while the exchange energy diverges for $L \rightarrow 0$, intersubband plasmons can still be reasonably described (apart from the fact that they drop below the p-h continuum,²⁶ which is an artifact of these functionals). In turn, intrasubband plasmon dispersions become suppressed and cease to exist, instead of approaching the limit of 2D plasmons.

In practice, it is important to know for what quantum well widths the 3D ALDA is still applicable. For instance, if $N_s = 10^{11} \text{ cm}^{-2}$ (which is a very typical value for many semiconductor quantum well samples), we find $L_{\text{crit}}^{\text{inter}} = 17 \text{ nm}$ for GaAs, which is rather narrow. Higher sheet densities allow one to push this limit to even narrower wells; and the breakdown for intrasubband dynamics occurs at even smaller well widths, as low as a few Å. This is certainly good news, considering the popularity of the ALDA and its ease of implementation. We also find that these values can be significantly higher for the PBE; in other words, using gradient-corrected xc functionals for quantum wells does not seem to pay off.

Clearly, the best option to describe the dynamics in strongly confined systems is using nonlocal orbital functionals such as PGG or ISTLS, since these are not tied to a particular choice of reference system (such as the 2D or 3D ALDA) and hence have no problem with dimensional crossover.

Finally, let us say a few words about correlation. In the ground-state,⁵⁻⁸ it was observed that local and semilocal correlation functionals break down in a similar manner as exchange functionals. This will also be the case for the dynamics. However, nonlocal, orbital-dependent correlation functionals are much more complicated than exchange functionals; for instance, implementing the ISTLS beyond exchange in linear response will remain a task for the future.

There is another aspect of correlation that is unique to the dynamical case, namely, it leads to dissipation of plasmon excitations even outside the particle-hole continuum. Plasmon damping in quantum wells has been studied within time-dependent current-DFT,³⁰⁻³³ using the complex and frequency-dependent xc kernel of Vignale and Kohn.^{34,35} This xc kernel is a local approximation of the current, and can lead to overdamping of charge plasmons.^{31,36} The effect is even more dramatic for spin plasmons, where the damping due to the spin Coulomb drag effect is significantly overestimated using a local approximation.³⁷ Again, it is found that the cure to this overdamping is provided by orbital functionals.³⁸

ACKNOWLEDGMENTS

This work was supported by DOE Grant No. DE-FG02-05ER46213.

Appendix A: The PBE exchange kernel

1. PBE exchange energy

The PBE exchange energy functional is defined as²⁰

$$E_x^{\text{PBE}}[n] = \int d^3r' e_x^h(n) \left[1 + \kappa - \frac{\kappa}{1 + \mu s^2/\kappa} \right]. \quad (\text{A1})$$

Here, the exchange energy density of a homogeneous 3D electron liquid of density n is

$$e_x^h(n) = -\frac{3c}{4} n^{4/3}, \quad c = \left(\frac{3}{\pi} \right)^{1/3}. \quad (\text{A2})$$

In Eq. (A1), $\kappa = 0.804$ and $\mu = 0.21951$ are parameters given in atomic units. The quantity s is defined as $s = |\nabla n|/2nk_F^{3D}$, where $k_F^{3D} = (3\pi^2 n)^{1/3}$ is the Fermi wavevector. Thus,

$$s = \frac{|\nabla n|}{2(3\pi^2)^{1/3} n^{4/3}}. \quad (\text{A3})$$

Putting this into Eq. (A1), we obtain

$$E_x^{\text{PBE}}[n] = \int d^3r' e_x^h(n) \left[1 + \kappa - \frac{\kappa}{1 + \gamma |\nabla n|^2/n^{8/3}} \right], \quad (\text{A4})$$

where $\gamma = (\mu/4\kappa)(3\pi^2)^{-2/3} = 0.007132$ a.u. For what follows, it is convenient to introduce the abbreviation

$$g(\mathbf{r}) = 1 + \gamma |\nabla n(\mathbf{r})|^2/n(\mathbf{r})^{8/3}. \quad (\text{A5})$$

2. PBE exchange potential

The PBE exchange potential in its spin-unresolved form is given by

$$\begin{aligned} v_x^{\text{PBE}}(\mathbf{r}) &= \frac{\delta E_x^{\text{PBE}}[n]}{\delta n(\mathbf{r})} \\ &= \int d^3r' \left(\frac{\delta e_x^h(n(\mathbf{r}'))}{\delta n(\mathbf{r})} \right) \left[1 + \kappa - \frac{\kappa}{g(\mathbf{r}')} \right] \\ &\quad - \int d^3r' e_x^h(n(\mathbf{r}')) \frac{\delta}{\delta n(\mathbf{r})} \left(\frac{\kappa}{g(\mathbf{r}')} \right). \end{aligned} \quad (\text{A6})$$

The first part is easy, with

$$\frac{\delta e_x^h(n(\mathbf{r}'))}{\delta n(\mathbf{r})} = -cn(\mathbf{r}')^{1/3} \delta(\mathbf{r}' - \mathbf{r}).$$

The second part requires more effort, involving functional derivatives of the gradient of n , which leads to gradients of delta functions. The final result is

$$\begin{aligned} v_x^{\text{PBE}}(\mathbf{r}) &= -cn(\mathbf{r})^{1/3} \left[1 + \kappa - \frac{\kappa}{g(\mathbf{r})} \right] \\ &\quad + \frac{3c}{4} n(\mathbf{r})^{-4/3} \nabla \left[\frac{2\kappa\gamma}{g(\mathbf{r})^2} \right] \cdot \nabla n(\mathbf{r}) \\ &\quad + \frac{3c}{4} n(\mathbf{r})^{-4/3} \frac{2\kappa\gamma}{g(\mathbf{r})^2} \nabla^2 n(\mathbf{r}). \end{aligned} \quad (\text{A7})$$

The spin-dependent version of the PBE exchange energy functional follows from the spin-scaling relation

$$E_x[n_\uparrow, n_\downarrow] = \frac{1}{2} E_x[2n_\uparrow] + \frac{1}{2} E_x[2n_\downarrow]. \quad (\text{A8})$$

This gives the spin-resolved exchange potential

$$v_{x\sigma}^{\text{PBE}}(\mathbf{r}) = v_x^{\text{PBE}}[2n_\sigma](\mathbf{r}). \quad (\text{A9})$$

For a system whose density is not spin polarized we have $n_\uparrow = n_\downarrow = n/2$. In this case, all potentials are the same, i.e., $v_{x\uparrow}^{\text{PBE}}(\mathbf{r}) = v_{x\downarrow}^{\text{PBE}}(\mathbf{r}) = v_x^{\text{PBE}}(\mathbf{r})$.

3. PBE exchange kernel

The parallel-spin exchange kernel is defined as follows:

$$f_{x,\sigma\sigma}^{\text{PBE}}(\mathbf{r}, \mathbf{r}') = \frac{\delta v_{x\sigma}^{\text{PBE}}(\mathbf{r})}{\delta n_\sigma(\mathbf{r}')} \quad (\text{A10})$$

(in the exchange-only case, the antiparallel-spin kernel is zero). For spin-unpolarized systems, we have

$$f_{x,\uparrow\uparrow}^{\text{PBE}}(\mathbf{r}, \mathbf{r}') = f_{x,\downarrow\downarrow}^{\text{PBE}}(\mathbf{r}, \mathbf{r}') = 2 f_x^{\text{PBE}}(\mathbf{r}, \mathbf{r}'), \quad (\text{A11})$$

where

$$f_x^{\text{PBE}}(\mathbf{r}, \mathbf{r}') = \frac{\delta v_x^{\text{PBE}}[n](\mathbf{r})}{\delta n(\mathbf{r}')} \quad (\text{A12})$$

After a rather lengthy calculation, one obtains

$$\begin{aligned} f_x^{\text{PBE}}(\mathbf{r}, \mathbf{r}') &= -\frac{c}{3} n(\mathbf{r})^{-2/3} \delta(\mathbf{r} - \mathbf{r}') \left[1 + \kappa - \frac{\kappa}{g(\mathbf{r})} \right] \\ &\quad - cn(\mathbf{r})^{1/3} \frac{\kappa\gamma}{g(\mathbf{r})^2} h(\mathbf{r}, \mathbf{r}') \\ &\quad - cn(\mathbf{r})^{-7/3} \delta(\mathbf{r} - \mathbf{r}') \nabla \left[\frac{2\kappa\gamma}{g(\mathbf{r})^2} \right] \cdot \nabla n(\mathbf{r}) \\ &\quad - \frac{3c}{4} n(\mathbf{r})^{-4/3} \nabla n(\mathbf{r}) \cdot \nabla \left(\frac{4\kappa\gamma^2}{g(\mathbf{r})^3} h(\mathbf{r}, \mathbf{r}') \right) \\ &\quad + \frac{3c}{4} n(\mathbf{r})^{-4/3} \nabla \left[\frac{2\kappa\gamma}{g(\mathbf{r})^2} \right] \cdot \nabla \delta(\mathbf{r} - \mathbf{r}') \\ &\quad - cn(\mathbf{r})^{-7/3} \delta(\mathbf{r} - \mathbf{r}') \frac{2\kappa\gamma}{g(\mathbf{r})^2} \nabla^2 n(\mathbf{r}) \\ &\quad + \frac{3c}{4} n(\mathbf{r})^{-4/3} \frac{2\kappa\gamma}{g(\mathbf{r})^2} \nabla^2 \delta(\mathbf{r} - \mathbf{r}') \\ &\quad - \frac{3c}{4} n(\mathbf{r})^{-4/3} \nabla^2 n(\mathbf{r}) \frac{4\kappa\gamma^2}{g(\mathbf{r})^3} h(\mathbf{r}, \mathbf{r}'), \end{aligned} \quad (\text{A13})$$

where we defined

$$h(\mathbf{r}, \mathbf{r}') = \frac{2\nabla n(\mathbf{r}) \cdot \nabla \delta(\mathbf{r} - \mathbf{r}')}{n(\mathbf{r})^{8/3}} - \frac{8|\nabla n(\mathbf{r})|^2}{3n(\mathbf{r})^{11/3}} \delta(\mathbf{r} - \mathbf{r}'). \quad (\text{A14})$$

To calculate excitation energies, one needs matrix elements of the exchange kernel. We here consider the case of quantum wells where everything becomes a function of z and z' , and we limit ourselves to intersubband excitations in the quasi-2D limit. Then, only the following matrix element is needed:

$$K_{12} = \int dz \int z' \varphi_1(z) \varphi_2(z) f_x^{\text{PBE}}(z, z') \varphi_1(z') \varphi_2(z'). \quad (\text{A15})$$

With the explicit form (A13) of the PBE exchange kernel, and abbreviating $\xi(z) = \varphi_1(z) \varphi_2(z)$, one obtains

$$\begin{aligned} K_{12} = & -\frac{c}{3} \int dz \xi(z)^2 n(z)^{-2/3} (1 + \kappa) \\ & + \frac{c\kappa}{3} \int dz \xi(z)^2 \frac{n(z)^{-2/3}}{g(z)} \\ & + 2c\kappa\gamma \int dz \xi(z) \frac{\partial}{\partial z} \left(\frac{\xi(z)n'(z)}{g(z)^2 n(z)^{7/3}} \right) \\ & + \frac{8c}{3} \kappa\gamma \int dz \xi(z)^2 \frac{n'(z)^2}{n(z)^{10/3} g(z)^2} \\ & - 2c\kappa\gamma \int dz \xi(z)^2 n(z)^{-7/3} n'(z) \frac{\partial}{\partial z} \left(\frac{1}{g(z)^2} \right) \\ & - 6c\kappa\gamma^2 \int dz \xi(z) \\ & \quad \times \frac{\partial}{\partial z} \left(\frac{n'(z) \frac{\partial}{\partial z} (\xi(z)n'(z)n(z)^{-4/3})}{g(z)^3 n(z)^{8/3}} \right) \\ & - 8c\kappa\gamma^2 \int dz \xi(z) \frac{n'(z)^2}{n(z)^{11/3} g(z)^3} \\ & \quad \times \frac{\partial}{\partial z} (\xi(z)n'(z)n(z)^{-4/3}) \\ & - \frac{3c}{2} \kappa\gamma \int dz \xi(z) \frac{\partial}{\partial z} \left[\xi(z)n(z)^{-4/3} \frac{\partial}{\partial z} \left(\frac{1}{g(z)^2} \right) \right] \\ & - 2c\kappa\gamma \int dz \xi(z)^2 \frac{n(z)^{-7/3}}{g(z)^2} n''(z) \\ & + \frac{3c}{2} \kappa\gamma \int dz \xi(z) \frac{\partial^2}{\partial z^2} \left(\frac{\xi(z)n(z)^{-4/3}}{g(z)^2} \right) \\ & + 6c\kappa\gamma^2 \int dz \xi(z) \frac{\partial}{\partial z} \left(\frac{\xi(z)n''(z)n'(z)}{n(z)^4 g(z)^3} \right) \\ & + 8c\kappa\gamma^2 \int dz \xi(z)^2 \frac{n''(z)(n'(z))^2}{n(z)^5 g(z)^3}. \quad (\text{A16}) \end{aligned}$$

Appendix B: The PGG kernel for quasi-2DEGs

In a quantum well of finite width, the single-particle orbitals have the form

$$\varphi_j(\mathbf{r}) = e^{i\mathbf{q}_{\parallel} \cdot \mathbf{r}_{\parallel}} \varphi_j(z), \quad (\text{B1})$$

where we ignore the normalization factor $A^{-1/2}$ for simplicity. The PGG exchange kernel (25) becomes

$$f_x^{\text{PGG}}(\mathbf{r}, \mathbf{r}') = -\frac{2}{|\mathbf{r} - \mathbf{r}'| n(z) n(z')} \times \left| \sum_{j=1}^{N_{\text{occ}}} \varphi_j(z) \varphi_j(z') \sum_{\mathbf{k}_{\parallel}} \theta(k_j - k_{\parallel}) e^{i\mathbf{k}_{\parallel} \cdot (\mathbf{r}_{\parallel} - \mathbf{r}'_{\parallel})} \right|^2 \quad (\text{B2})$$

where $k_j = \sqrt{2(\varepsilon_F - \varepsilon_j)}$. Carrying out the integral over \mathbf{k}_{\parallel} , and defining $\rho_{\parallel} = \mathbf{r}_{\parallel} - \mathbf{r}'_{\parallel}$, one finds

$$f_x^{\text{PGG}}(\mathbf{r}, \mathbf{r}') = -\frac{2}{|\mathbf{r} - \mathbf{r}'| n(z) n(z')} \times \left| \sum_{j=1}^{N_{\text{occ}}} \varphi_j(z) \varphi_j(z') \frac{k_j J_1(k_j \rho_{\parallel})}{2\pi \rho_{\parallel}} \right|^2, \quad (\text{B3})$$

where J_1 denotes a standard Bessel function. Fourier transformation with respect to ρ_{\parallel} yields

$$f_x^{\text{PGG}}(q_{\parallel}, z, z') = -\sum_{j,l}^{N_{\text{occ}}} k_j k_l \frac{\varphi_j(z) \varphi_l(z) \varphi_j(z') \varphi_l(z')}{\pi n(z) n(z')} \times \int_0^{\infty} d\rho_{\parallel} \frac{J_0(q_{\parallel} \rho_{\parallel}) J_1(k_j \rho_{\parallel}) J_1(k_l \rho_{\parallel})}{\rho_{\parallel} \sqrt{\rho_{\parallel}^2 + (z - z')^2}}. \quad (\text{B4})$$

If only the first subband is occupied, this simplifies to

$$f_x^{\text{PGG}}(q_{\parallel}, z, z') = -\frac{2}{N_s} \int_0^{\infty} d\rho_{\parallel} \frac{J_0(q_{\parallel} \rho_{\parallel}) J_1^2(k_1 \rho_{\parallel})}{\rho_{\parallel} \sqrt{\rho_{\parallel}^2 + (z - z')^2}}. \quad (\text{B5})$$

In the limit of a pure 2DEG, the PGG exchange kernel thus becomes

$$f_{x,2\text{D}}^{\text{PGG}}(q_{\parallel}) = -\frac{2}{n_{2\text{D}}} \int_0^{\infty} \frac{d\rho_{\parallel}}{\rho_{\parallel}^2} J_0(q_{\parallel} \rho_{\parallel}) J_1^2(k_F^{\text{2D}} \rho_{\parallel}). \quad (\text{B6})$$

Let us mention that the PGG exchange kernel (25) can also be written as

$$f_x^{\text{PGG}}(\mathbf{r}, \mathbf{r}') = 2 \frac{g_0(\mathbf{r}, \mathbf{r}') - 1}{|\mathbf{r} - \mathbf{r}'|}, \quad (\text{B7})$$

where $g_0(\mathbf{r}, \mathbf{r}')$ is the noninteracting pair correlation function. One then finds the following alternative form of the PGG exchange kernel for a 2DEG:

$$f_{x,2\text{D}}^{\text{PGG}}(q_{\parallel}) = -\frac{\pi}{q_{\parallel}} G_{\uparrow\uparrow}^{\text{S}}(q_{\parallel}), \quad (\text{B8})$$

where

$$\begin{aligned} G_{\uparrow\uparrow}^{\text{S}}(q_{\parallel}) &= -\frac{q_{\parallel}}{2\pi^2 n} \int \frac{d^2 q'_{\parallel}}{|\mathbf{q}_{\parallel} - \mathbf{q}'_{\parallel}|} [S_0(q'_{\parallel}) - 1] \\ &= -\frac{2q_{\parallel}}{\pi^2 n} \int_0^{\infty} \frac{q'_{\parallel} dq'_{\parallel}}{q_{\parallel} + q'_{\parallel}} K \left(\frac{\sqrt{4q_{\parallel} q'_{\parallel}}}{q_{\parallel} + q'_{\parallel}} \right) [S_0(q'_{\parallel}) - 1] \end{aligned} \quad (\text{B10})$$

is the so-called Slater local field factor (S_0 is the noninteracting static structure factor and K is the complete elliptic integral of the first kind).⁴

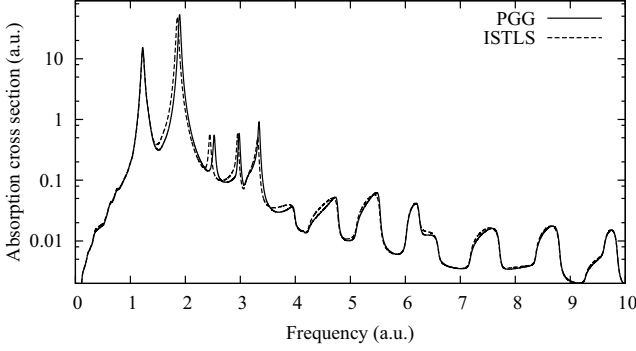


FIG. 9. Photoabsorption cross section for $q_{\parallel} = 0$ intersubband charge plasmons, for a quantum well with 5 occupied subbands, comparing PGG and exchange-only ISTLS.

Appendix C: ISTLS in the exchange-only limit

In the inhomogeneous STLS (ISTLS) approach, the xc kernel has the following tensorial form:^{9,10}

$$f_{xc,\mu\nu}^{\text{ISTLS}}(\mathbf{r}, \mathbf{r}') = -\frac{2}{\omega^2} [g(\mathbf{r}, \mathbf{r}') - 1] \frac{\partial}{\partial \mu} \frac{1}{|\mathbf{r} - \mathbf{r}'|} \frac{\partial}{\partial \nu}, \quad (\text{C1})$$

where μ, ν denote Cartesian coordinates and $g(\mathbf{r}, \mathbf{r}')$ is the pair correlation function. The exchange-only limit of this expression is obtained by using the noninteracting pair correlation function, which yields

$$f_{xc,\mu\nu}^{\text{ISTLS}}(\mathbf{r}, \mathbf{r}') = 2 \frac{\left| \sum_{j=1}^{N_{\text{occ}}} \varphi_j(\mathbf{r}) \varphi_j^*(\mathbf{r}') \right|^2}{\omega^2 n(\mathbf{r}) n(\mathbf{r}')} \frac{\partial}{\partial \mu} \frac{1}{|\mathbf{r} - \mathbf{r}'|} \frac{\partial}{\partial \nu}. \quad (\text{C2})$$

We consider the case of a quantum well with finite width, where the Kohn-Sham orbitals have the form (B1), and we limit ourselves to plasmon modes with in-plane wavevector $q_{\parallel} = 0$, so that the dynamics is uniform within the plane of the well and, hence, effectively

one-dimensional. Then, only the zz component of the tensorial xc kernel is relevant, and it is straightforward to transform it to a scalar exchange kernel.¹² Using the same notation as in Appendix B, we obtain

$$f_x^{\text{ISTLS}}(q_{\parallel} = 0, z, z') = \int_z^{\infty} dz_1 \int_0^{\infty} \frac{d\rho_{\parallel}}{\rho_{\parallel}} \times \frac{\left| \sum_j^{N_{\text{occ}}} \varphi_j^*(z_1) \varphi_j(z') k_j J_1(k_j \rho_{\parallel}) \right|^2}{\pi n(z_1) n(z')} \times \left(\frac{\partial}{\partial z_1} \frac{1}{\sqrt{\rho_{\parallel}^2 + (z_1 - z')^2}} \right). \quad (\text{C3})$$

Comparing with Eq. (B4) [notice that $J_0(0) = 1$], we can rewrite this as

$$f_x^{\text{ISTLS}}(0, z, z') = f_x^{\text{PGG}}(0, z, z') - \int_z^{\infty} dz_1 \int_0^{\infty} \frac{d\rho_{\parallel}}{\rho_{\parallel}} \times \sum_{l,m}^{N_{\text{occ}}} \frac{k_l k_m J_1(k_l \rho_{\parallel}) J_1(k_m \rho_{\parallel})}{\sqrt{\rho_{\parallel}^2 + (z_1 - z')^2}} \times \frac{\partial}{\partial z_1} \left(\frac{\varphi_l(z_1) \varphi_l^*(z') \varphi_m^*(z_1) \varphi_m(z')}{\pi n(z_1) n(z')} \right) \quad (\text{C4})$$

It thus turns out that the ISTLS exchange kernel is equal to the PGG exchange kernel plus a correction term. If only the lowest subband is occupied ($N_{\text{occ}} = 1$), the correction term vanishes because then the derivative with respect to z_1 gives zero.

Figure 9 gives a comparison of PGG and ISTLS for the case of a quantum well with 5 occupied subbands. The figure shows the frequency-dependent photoabsorption cross section corresponding the intersubband charge plasmons. As can be seen, the difference between PGG and ISTLS is marginal.

¹ P. Hohenberg and W. Kohn, Phys. Rev. **136**, B864 (1964).
² W. Kohn and L. J. Sham, Phys. Rev. **140**, A1133 (1965).
³ The usual Coulomb interaction, $1/|\mathbf{r} - \mathbf{r}'|$, applies in 3D and 2D, but in 1D it would lead to divergencies and requires regularization (see Ref. 4).
⁴ G. F. Giuliani and G. Vignale, *Quantum Theory of the Electron Liquid* (Cambridge University Press, 2005).
⁵ L. Pollack and J. P. Perdew, J. Phys.: Condens. Matter **12**, 1239 (2000).
⁶ Y.-H. Kim, I.-H. Lee, S. Nagaraja, J.-P. Leburton, R. Q. Hood, and R. M. Martin, Phys. Rev. B **61**, 5202 (2000).
⁷ L. A. Constantin, J. P. Perdew, and J. M. Pitarke, Phys. Rev. Lett. **101**, 016406 (2008).
⁸ L. A. Constantin, Phys. Rev. B **78**, 155106 (2008).
⁹ J. F. Dobson, J. Wang, and T. Gould, Phys. Rev. B **66**, 081108 (2002).

¹⁰ J. F. Dobson, Phys. Chem. Chem. Phys. **11**, 4528 (2009).
¹¹ E. Runge and E. K. U. Gross, Phys. Rev. Lett. **52**, 997 (1984).
¹² C. A. Ullrich, *Time-dependent density-functional theory: Concepts and applications* (Oxford University Press, 2012).
¹³ C. A. Ullrich and Zeng-hui Yang, Brazilian J. Phys. **44**, 154 (2014).
¹⁴ M. Petersilka, U. J. Gossmann, and E. K. U. Gross, Phys. Rev. Lett. **76**, 1212 (1996).
¹⁵ M. E. Casida, in *Recent Advances in Density Functional Methods*, edited by D. E. Chong, Vol. 1 of *Recent Advances in Computational Chemistry* (World Scientific, Singapore, 1995), p. 155.
¹⁶ In this paper we distinguish quasi-2D and strictly 2D systems. By quasi-2D we mean the quantum limit in which all electrons occupy the lowest subband in the well, but the

- electron density distribution still has a finite lateral width; strictly 2D implies the limit in which the width has become infinitesimal.
- ¹⁷ J. H. Davies, *The Physics of Low-Dimensional Semiconductors* (Cambridge University Press, 1998).
 - ¹⁸ P. Harrison, *Quantum wells, wires and dots*, 2nd Edition (Wiley, Chichester, 2005).
 - ¹⁹ E. K. U. Gross and W. Kohn, Phys. Rev. Lett. **55**, 2850 (1985); Erratum: *ibid.* **57**, 923 (1986).
 - ²⁰ J. P. Perdew, K. Burke, and M. Ernzerhof, Phys. Rev. Lett. **77**, 3865 (1996); Erratum: *ibid.* **78**, 1396 (1997).
 - ²¹ M. Petersilka, U. J. Gossmann, and E. K. U. Gross, in *Electronic density functional theory: recent progress and new directions*, ed. by J. F. Dobson and G. Vignale (Plenum, New York, 1998), p. 177.
 - ²² N. H. March and M. P. Tosi, Adv. Phys. **44**, 299 (1995).
 - ²³ J. F. Dobson, Phys. Rev. B **46**, 10163 (1992).
 - ²⁴ W. L. Schaich and J. F. Dobson, Phys. Rev. B **49**, 14700 (1994).
 - ²⁵ A. Liebsch, *Electronic excitations at metal surfaces* (Plenum Press, New York, 1997).
 - ²⁶ A similar effect was described earlier by DasSarma and Marmorkos [Phys. Rev. B **47**, 16343 (1993)], but it was not recognized as being an artifact of the 3D ALDA in the quasi-2D limit.
 - ²⁷ A. Savin, C. J. Umrigar, and X. Gonze, Chem. Phys. Lett. **288**, 391 (1998).
 - ²⁸ K. Burke, M. Petersilka, and E. K. U. Gross, in *Recent Advances in Density Functional Methods*, ed. V. Barone, A. Bencini, and P. Fantucci, Vol. III (World Scientific, Singapore, 2002), p. 67.
 - ²⁹ However, there are molecular examples where the exact Kohn-Sham transitions do not lie between the singlet and triplet excitations, see E. J. Baerends, O. V. Gritsenko, and R. van Meer, Phys. Chem. Chem. Phys. **15**, 16408 (2013).
 - ³⁰ C. A. Ullrich and G. Vignale, Phys. Rev. B **58**, 7141 (1998).
 - ³¹ C. A. Ullrich and G. Vignale, Phys. Rev. B **58**, 15756 (1998).
 - ³² C. A. Ullrich and G. Vignale, Phys. Rev. Lett. **87**, 037402 (2001).
 - ³³ C. A. Ullrich and G. Vignale, Phys. Rev. B **65**, 245102 (2002); Erratum: *ibid.* **70**, 239903(E) (2004).
 - ³⁴ G. Vignale and W. Kohn, Phys. Rev. Lett. **77**, 2037 (1996).
 - ³⁵ G. Vignale, C. A. Ullrich, and S. Conti, Phys. Rev. Lett. **79**, 4878 (1997).
 - ³⁶ R. D'Agosta, M. Di Ventura and G. Vignale, Phys. Rev. B **76**, 035320 (2007).
 - ³⁷ I. D'Amico and C. A. Ullrich, Phys. Rev. B **74**, 121303 (2006).
 - ³⁸ I. D'Amico and C. A. Ullrich, Phys. Rev. B **88**, 155324 (2013).